Energy Optimum Reactionless Path Planning for Capture of Tumbling Orbiting Objects using a Dual-Arm Robot

S. V. Shah and A. Gattupalli
Robotics Research Center
International Institute of Information Technology
Hyderabad 500032, India
surilshah@iiit.ac.in, gattupalliaditya@gmail.com

A. K. Misra
Mechanical Engineering Department
McGill University
Montreal, QCH3A0C3, Canada
arun.misra@mcgill.ca

***Abstract*—This paper presents energy optimum capture of orbiting objects using a dual-arm robot mounted on a service satellite. An attempt has been made to formulate energy efficient trajectories for the dual-arm robot such that the reaction moments acting on the base satellite are minimum. To achieve this, first a local optimization problem is formulated exploiting redundancy associated with the constraints for reactionless manipulation. This method, however, fails to provide optimal trajectories. In order to overcome this disadvantage, an optimal control problem is formulated which not only helps in achieving energy efficient trajectories but also ensures zero reaction moments to the base satellite. The proposed method is validated using a 6-link planar dual-arm robot mounted on a service satellite.**

Keywords – Reactionless manipulation; space robot; optimal path planning

I. INTRODUCTION

In recent years, there has been a substantial growth in the number of satellites deployed in space. Due to this continuous growth, on-orbit services such as refuelling and servicing of orbiting satellites, capture of space debris, etc. will be an integral part of space missions in the future [1], [2]. These operations will be carried out autonomously using a robotic system mounted on a service satellite. Unlike a fixed-base ground robot, a space robot causes disturbances to the base of the satellite due to their coupled dynamics. A space robot also has constraints on the energy usage for servicing purpose.

It is essential for a space robot to perform on-orbit servicing while minimising the base attitude disturbances. This is due to the fact that attitude disturbances can destabilise the satellite and may cause damage to its internal hardware. Use of thruster for attitude control will require fuel consumption which is reserved mainly for orbital manoeuvres. Hence, several researchers have focused on robotic manipulation with minimum or no change in the attitude of the base satellite. This is also known as reactionless manipulation of robotic arm. In [3], [4] disturbance maps were used to minimise base attitude motion but were not able to completely eliminate them. Another reactionless manipulation technique using a Reaction Null Space (RNS) led to zero attitude disturbances of the base satellite [5] which was subsequently validated on the ETS VII space robot [6]. However, these techniques for minimising attitude disturbances do not take into account the energy consumed by the manipulator during orbital servicing.

It is worth noting that the energy generated by satellite mounted solar panels should be used wisely as it is to be shared with other on-board satellite hardware, whereas fuel is reserved mainly for orbital manoeuvres. Therefore, reactionless trajectories of robot should also be optimum from the point of view of energy consumption. Some research efforts have been made to address the problem of optimal trajectory planning of a space robot. Global optimal path planning for a space robot was discussed in [7] which optimises the Euclidean velocity norm. In [8], [9] optimal planning was achieved by optimizing the satellite base torques and the operation time, respectively. These optimization methods were not able to completely eliminate the base attitude disturbances.

Optimal trajectory planning minimising the time and relative velocity between the end-effector and the target was proposed in [10]. A method for optimal control which minimised target capture time [11] was later extended to minimise the reaction torques acting on the base satellite [12]. Robust control of a space robot taking into account the uncertainties in the dynamics of the satellite and the space object was considered in [13], [14]. However, these methods focused on either reducing the operation time or base reactions ignoring the energy usage.

Moreover, in the above works autonomous capture was carried out using a single-arm robotic system. Orbital capture with single arm is difficult when there is no provision for the grapple fixture or the object is tumbling. A dual-arm robotic system for reactionless manipulation was presented in [15] which used one arm to perform the desired task while the other arm compensated for base inertial motion. In [16], [17] the coordinated motion planning of a spatial dual-arm space robot for target capture was presented without taking into account the base attitude disturbances. Recently in [18], point-to-point path planning strategies of reactionless capture using a planar dual-arm was presented without emphasizing the energy requirement. Energy optimal reactionless path planing for dual-arm robot is not reported in literature, to the best of the authors' knowledge.

Planning such motions for the dual-arm robotic system for capture of tumbling object is challenging due to non-holonomic nature of the constraints for reactionless manipulation, and coupled dynamics of the arms. It is also desired that the robot is manipulated in such a way that there is minimum impact during capture. This makes path planning even more complex. In the present work, an energy optimal path planning strategy to capture orbiting objects using a dual-arm robot mounted on a satellite with zero attitude disturbance is proposed. This makes fundamental contribution to the proposed problem. The proposed method uses optimal control in conjunction with redundancy formalism in order to achieve energy efficient reactionless manipulation.

The rest of the paper is organized as follows: Section 2 presents mathematical preliminaries. Section 3 illustrates reactionless path planning of a dual-arm robot. Energy optimum path planning is presented in Section 4. Finally, conclusions are given in Section 5.

II. Mathematical Preliminaries

For an n-Degrees-Of-Freedom (n-DOF) robotic system mounted on a floating-base, linear momentum ($\boldsymbol{p}$) and angular momentum ($\boldsymbol{l}$) are given by [6]

$$\begin{bmatrix} \boldsymbol{p} \\ \boldsymbol{l} \end{bmatrix} = \boldsymbol{I}_b \dot{\boldsymbol{t}}_b + \boldsymbol{I}_{bm} \dot{\boldsymbol{\theta}}, \tag{1}$$

where $\boldsymbol{I}_b \in R^{6\times 6}$ is the inertia matrix of the floating-base, $\boldsymbol{I}_{bm} \in R^{6\times n}$ is the coupling inertia matrix, $\dot{\boldsymbol{t}}_b \in R^6$ is the twist vector containing linear velocity ($\boldsymbol{v}_0$) and angular velocity ($\boldsymbol{\omega}_0$) of the base, and $\dot{\boldsymbol{\theta}} \in R^n$ is the vector of joint velocities. The expression for the angular momentum $\boldsymbol{l}$ in (1) can also be reformulated only in terms of $\boldsymbol{\omega}_0$ as [6]

$$\boldsymbol{l} = \tilde{\boldsymbol{I}}_b \boldsymbol{\omega}_0 + \tilde{\boldsymbol{I}}_{bm} \dot{\boldsymbol{\theta}}. \tag{2}$$

Note that in (1), $\boldsymbol{I}_{bm}\dot{\boldsymbol{\theta}}$ is referred to as the coupling momentum, whereas $\tilde{\boldsymbol{I}}_{bm}\dot{\boldsymbol{\theta}}$ in (2) is referred to as the coupling angular momentum. The above expression forms foundation for derivation of the constraints for reactionless manipulation.

Constraints for reactionless manipulation

The angular momentum of (2) is conserved if no external forces are acting on a system. Moreover, if the system starts from the rest then $\boldsymbol{l} = \boldsymbol{0}$, and (2) can be rewritten as

$$\tilde{\boldsymbol{I}}_b \boldsymbol{\omega}_0 + \tilde{\boldsymbol{I}}_{bm} \dot{\boldsymbol{\theta}} = 0. \tag{3}$$

If stationary state of the attitude of the base is maintained, i.e., $\boldsymbol{\omega}_0 = 0$, then

$$\tilde{\boldsymbol{I}}_{bm} \dot{\boldsymbol{\theta}} = \boldsymbol{0}. \tag{4}$$

The above equation ensures zero attitude disturbance. Note that the satellite is free to move along Cartesian axes. Henceforth, the reactionless manipulation imply motion with zero attitude disturbance. Planning motion in the task space using (4) is a complex problem. Hence, these constraints are converted into task-level constraints i.e., in the space of the end-effector, using a Generalized Jacobian Matrix (GJM) [20] which relates end-effector velocities ($\dot{\boldsymbol{t}}_e$) relative to the inertial frame of reference, and joint rates as

$$\dot{\boldsymbol{t}}_e = \boldsymbol{J}_g \dot{\boldsymbol{\theta}}, \ where \ \boldsymbol{J}_g = \left(\boldsymbol{J}_{me} - \boldsymbol{J}_{be} \boldsymbol{I}_b^{-1} \boldsymbol{I}_{bm} \right). \tag{5}$$

In (5), $\boldsymbol{J}_{be}$and $\boldsymbol{J}_{me}$ are the Jacobian matrices for the base and manipulator [18], respectively, and $\boldsymbol{J}_g$ is the Generalized Jacobian Matrix (GJM). The GJM can be interpreted similar to the Jacobian for an earth-based robot $(i.e., simply\ \boldsymbol{J}_{me})$; however here, $\boldsymbol{J}_g$ contains several terms associated with system's dynamics. Substituting $\dot{\boldsymbol{\theta}}$ from (5) into (4) one gets the task-level constraints, i.e.,

$$\tilde{\boldsymbol{I}}_{be} \dot{\boldsymbol{t}}_e = \boldsymbol{0}, \tag{6}$$

where $\tilde{\boldsymbol{I}}_{be} = \tilde{\boldsymbol{I}}_{bm} \boldsymbol{J}_g^{-1}$; pseudo inverse can be used if necessary. The Degree-of-Redundancy (DOR), r, associated with (6) is given by the difference between the number of rows and columns of $\tilde{\boldsymbol{I}}_{be}$, and solution of (6) lies in the r-dimensional subspace of R^n. Solution of (6) can be obtained either using pseudo inverse [6] or co-ordinate partitioning [18]. The latter approach is preferred here as it allows one to specify some velocities of the end-effectors in independent manner.

III. Reactionless Path Planning of a Dual-arm Robot

In this section reactionless path planing for the dual-arm robotic system is discussed for capture of a tumbling orbiting object. Co-ordinate partitioning is used here to obtain solution of (6). For this, the end-effector's velocity space is partitioned into independent velocity ($\dot{\boldsymbol{t}}_e^i$) and dependent velocity ($\dot{\boldsymbol{t}}_e^d$) components as

$$\begin{bmatrix} \tilde{\boldsymbol{I}}_{be}^d & \tilde{\boldsymbol{I}}_{be}^i \end{bmatrix} \begin{bmatrix} \dot{\boldsymbol{t}}_e^d \\ \dot{\boldsymbol{t}}_e^i \end{bmatrix} = \boldsymbol{0} \ . \tag{7}$$

Note that the maximum number of independent co-ordinates in (7) are limited to DOR. If we choose the number

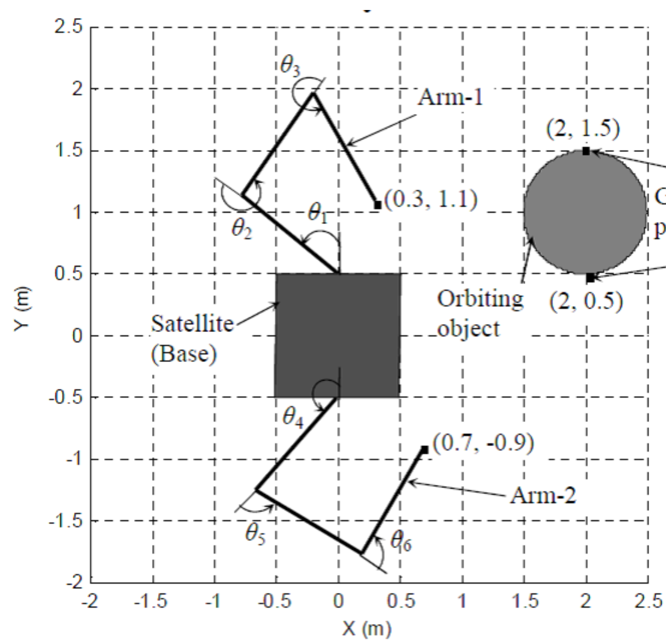

Fig. 1. Planar dual-arm robot mounted on a satellite

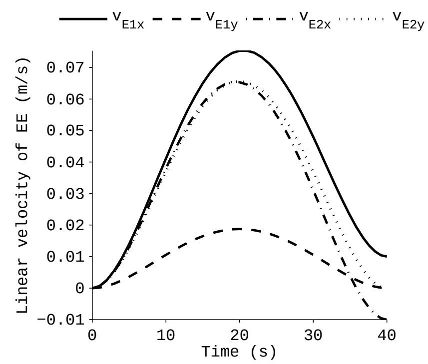

Fig. 2. Independent velocities

of independent velocities equal to DOR then the dependent velocities are uniquely given by

$$\dot{\boldsymbol{t}}_e^d = -\tilde{\boldsymbol{I}}_{be}^{d^{-1}} \tilde{\boldsymbol{I}}_{be}^i \dot{\boldsymbol{t}}_e^i. \quad (8)$$

If the number of independent velocities are chosen less than DOR then the dependent velocities can be expressed as

$$\dot{\boldsymbol{t}}_e^d = -\tilde{\boldsymbol{I}}_{be}^{d+} \tilde{\boldsymbol{I}}_{be}^i \dot{\boldsymbol{t}}_e^i + (\boldsymbol{E} - \tilde{\boldsymbol{I}}_{be}^{d+} \tilde{\boldsymbol{I}}_{be}^d)\dot{\boldsymbol{\zeta}}, \quad (9)$$

where $(\boldsymbol{E} - \tilde{\boldsymbol{I}}_{be}^{d+} \tilde{\boldsymbol{I}}_{be}^d)$ is the null space projector and $\dot{\boldsymbol{\zeta}}$ is an arbitrary velocity vector. The second term in (9) allows one to use free DOR for control of secondary tasks such as singularity avoidance, collision avoidance, energy minimization, etc. In this section, path planing is first carried out using (9). The designed end-effectors trajectories are then used to obtain the joint space trajectories using the inverse of the GJM.

In the case of planar a 6-DOF planar dual-arm space robot shown in Fig. 1, the DOR is equal to 5, and hence, maximum 5 velocities can be chosen independently out of six. Here, four linear velocities of the end-effectors, i.e., v_{1x}, v_{1y}, v_{2x} and v_{2y}, are chosen independently whereas ω_{1z} and ω_{2z} are assumed to be the dependent velocities. The choice of these independent velocities is obvious as the objective is to intercept the grapple points with desired linear velocity in order to minimize impact at the capture instant. In order to design the independent velocities, first, position level trajectory is designed similar to 3-4-5 polynomial in [21], however with given initial and final velocities, as

$$x(t) = x_I + T\Big[a\Big(\frac{t}{T}\Big) + b\Big(\frac{t}{T}\Big)^3 + c\Big(\frac{t}{T}\Big)^4 + d\Big(\frac{t}{T}\Big)^5\Big], \quad (10)$$

where $a = \dot{x}_I, b = 10v - (6\dot{x}_I + 4\dot{x}_F), c = -15v + (8\dot{x}_I + 7\dot{x}_F), d = 6v - (3\dot{x}_I + 3\dot{x}_F)$ and $v = [x_F - x_I]/T$. Moreover, (x_I and x_F) and ($\dot{x}_I$ and $\dot{x}_F$) are the initial and final positions and velocities, respectively. Zero initial and final accelerations are assumed for designing the above trajectory. Differentiating (10), the expression for independent velocities as fourth order polynomials is obtained as

$$\dot{x}(t) = a + 3b\Big(\frac{t}{T}\Big)^2 + 4c\Big(\frac{t}{T}\Big)^3 + 5d\Big(\frac{t}{T}\Big)^4. \quad (11)$$

Given the independent velocities, the dependent velocities are obtained from (9).

TABLE I. MODEL PARAMETERS FOR SATELLITE AND DUAL-ARM

	Satellite	Arm-1 and 2		
		Link-1	Link-2	Link-3
$mass(Kg)$	500	10	10	10
$length(m)$	1	1	1	1
$I_{zz}(Kg.m^2)$	83.61	1.05	1.05	1.05

This is illustrated next using the planar dual-arm robotic system mounted on a satellite, as shown in Fig. 1. Each arm is comprised of three rigid links and 3-DOF. The centre-of-mass of the satellite and orbiting object lie at $(0m, 0m)$, and $(2m, 1m)$, respectively. The dual arms are initially in a non-symmetric configuration, as in practice it is not possible to achieve perfect symmetry. The points to be grappled on the object are also shown in Fig. 1. The model parameters of the satellite and dual-arm are given in Table I. The object is assumed to be rotating with constant angular velocity relative to satellite. The arm-1 and -2 start from rest and are required to intercept the target with linear velocity (-0.01 m/s, 0 m/s) and (0.01 m/s, 0 m/s), respectively. The independent velocities for this are designed using (11), and are shown in Fig. 2. The dependent velocities are then

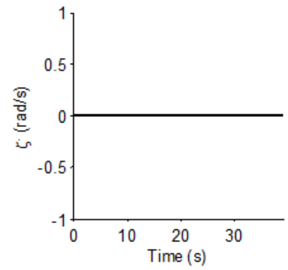

(a) Zeta

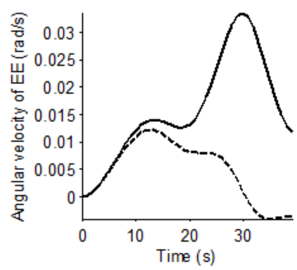

(b) Endeffectors' angular velocity

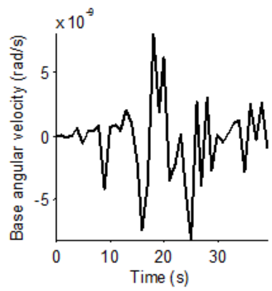

(c) Base angular velocity

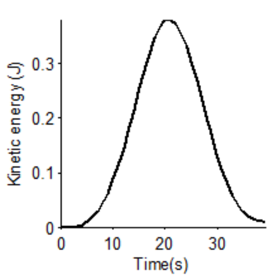

(d) Kinetic energy

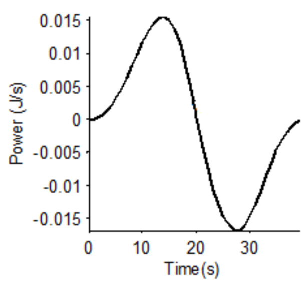

(e) Power

Fig. 3. Results of reactionless manipulation

obtained from (9). For this the value of $\dot{\boldsymbol{\zeta}}$ is assumed to be [0 0]^T. The dependent velocities are shown Fig. 3(b). Figure 3(c) shows that the angular velocity of the base satellite is of order $10^{-9} rad/s$ which ensures reactionless manipulation. Energy and power requirement are also shown in Figs. 3(d) and 3(e), respectively. They correspond to the assumed value of $\dot{\boldsymbol{\zeta}}$ =[0 0]^T, and are not the optimal ones. The results are obtained using the space robot module of Recursive Dynamics Simulator (ReDySim) [22], developed by the first author.

IV. Energy Optimal Reactionless Path Planning

The reactionless path planning strategy presented in the previous subsection is not optimal from the energy point of view. It is worth noting that path planned using (9) has free DOR and allows one to obtain several reactionless paths for different combinations of $\dot{\boldsymbol{\zeta}}$. In this section two optimization methods are discussed for energy optimal reactionless path planning.

A. *Local optimization*

In this approach, one free DOR associated with (9) is used to obtain energy optimal path planing. For this, the value of $\dot{\boldsymbol{\zeta}}$ which minimize a desired cost function at each time instant is obtained using constrained optimization. As the objective is to minimize energy consumption, cost function is taken as

$$C = \dot{\boldsymbol{\theta}}^T \boldsymbol{I}_m \dot{\boldsymbol{\theta}}, \tag{12}$$

where $\dot{\boldsymbol{\theta}}^T \boldsymbol{I}_m \dot{\boldsymbol{\theta}}$ is the instantaneous kinetic energy of the system under study. Therefore, a local optimization problem is formulated as

$$\dot{\boldsymbol{\zeta}} = \arg\min_{\dot{\boldsymbol{\zeta}}} (\dot{\boldsymbol{\theta}}^T \boldsymbol{I}_m \dot{\boldsymbol{\theta}}), \tag{13}$$

where

$$\dot{\boldsymbol{\theta}} = \boldsymbol{J}_g{}^{-1} \dot{\boldsymbol{t}}_e(\dot{\boldsymbol{\zeta}}). \tag{14}$$

In (14), $\dot{\boldsymbol{t}}_e$ is obtained from (9). Optimization is carried out using $fminunc$ of MATLAB which finds minimum of an unconstrained multivariable function, and uses BFGS Quasi-Newton method with a cubic line search procedure. The results of local optimization are shown in Fig. 4. It can be seen that the robot moves in reactionless manner (Fig. 4(c)), however, both energy (Fig. 4(d)) and total power (Fig. 4(e)) requirements are higher in comparison to the same obtained Fig. 3. in the case of local optimization. In order to get further insight, values of $\dot{\boldsymbol{\zeta}}$ and dependent angular velocities are also plotted in Figs. 4(a) and Fig. 4(b). It can be seen that at $t = 18sec$ there is a sudden change in the optimal value of $\dot{\boldsymbol{\zeta}}$. This results into significant change in the value of dependent velocity requiring increase in the energy consumption. This is mainly due to the fact that the local optimization gives a value of $\dot{\boldsymbol{\zeta}}$ which only minimizes instantaneous energy at the given time instant. This does not ensure minimization of the total energy over the entire time period. Therefore, even though the local optimization minimizes the value of the cost function for a given time instant, this value could still be high in comparison to the same at other time instances. Thus, local optimization fails to provide energy optimal path due to nonholonomic nature of the constraints in (9). In order to overcome this disadvantage an optimal control problem is formulated next.

B. *Optimal control*

As discussed in the previous subsection local optimization failed to provide minimization of the total energy. Optimal control provides global optimization, and hence, allows to minimize total energy over the given time interval. Optimal control problem includes a cost functional which is a function of state and control variables. In this work cost function is defined as an integral of instantaneous kinetic energy for given time interval, i.e.,

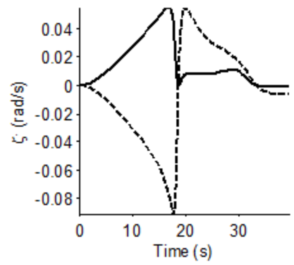

(a) Zeta

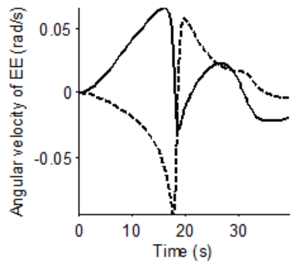

(b) Endeffectors' angular velocity

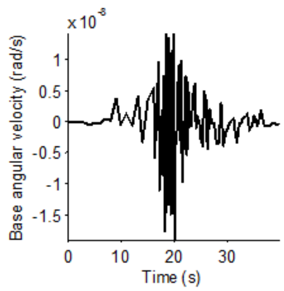

(c) Base angular velocity

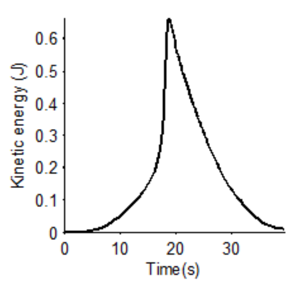

(d) Kinetic energy

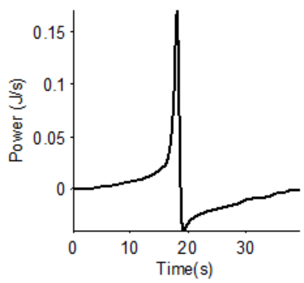

(e) Power

Fig. 4. Results of local optimization

$$C = \int_{t_i}^{t_f} \dot{\boldsymbol{\theta}}^T \boldsymbol{I}_m \dot{\boldsymbol{\theta}} \, dt, \tag{15}$$

where t_i and t_f are initial and final times, respectively. Next, the optimal control problem is formulated as

$$\dot{\boldsymbol{\zeta}} = \arg\min_{\dot{\boldsymbol{\zeta}}} \left(\int_{t_i}^{t_f} \dot{\boldsymbol{\theta}}^T \boldsymbol{I}_m \dot{\boldsymbol{\theta}} \, dt \right). \tag{16}$$

The above function is subject to the reactionless constraints, i.e., $\dot{\boldsymbol{\theta}} = \boldsymbol{J}_g{}^{-1} \dot{\boldsymbol{t}}_e(\dot{\boldsymbol{\zeta}})$ with the control input being $\dot{\boldsymbol{\zeta}}$. Apart from this equality constraints there are also bounds on the joint angles and the control inputs. Solution of the above formulated problem is obtained using both ReDySim and optimal control module of TOMLAB [23] which gives the optimal value of $\dot{\boldsymbol{\zeta}}$. Here, the system is represented by a set of ordinary differential equations in the state-space form. The optimal control problem is solved using

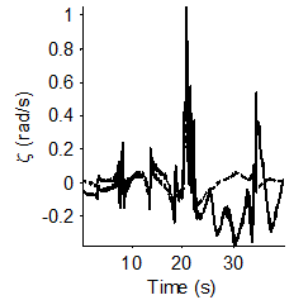

(a) Zeta

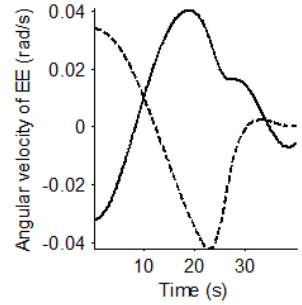

(b) Endeffectors' angular velocity

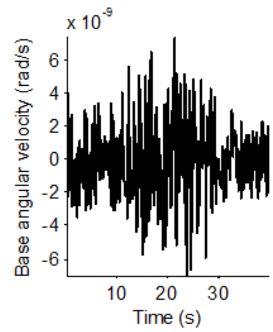

(c) Base angular velocity

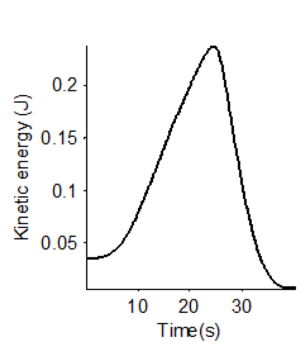

(d) Kinetic energy

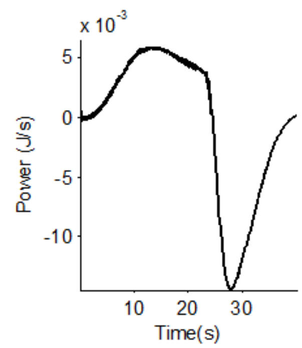

(e) Power

Fig. 5. Results of optimal control

pseudospectral collocation methods. The solution takes the form of a polynomial, and this polynomial satisfies the equation and the path constraints at the collocation points. Gauss points are chosen as the collocation points. Note that even though the method does not use Pontryagin's maximum principle, the results are mathematically equivalent.

Optimal control is performed next for the reactionless manipulation of the dual-arm from initial positions to grapple points as shown in Fig. 1. Results of optimal control are depicted in Fig. 5. Figures 5(d) and 5(e) show energy and power requirements. It is evident that both energy and power requirements are much lower than those obtained in Fig. 3 and Fig. 4. It can also be seen from Figs. 5(a) and 5(b) that the values of $\dot{\zeta}$, obtained from optimal control, resulted into smooth transition in the dependent angular velocities. The base angular velocity shown in Fig. 5(c) is of the order $10^{-9} rad/s$, which ensures reactionless manipulation of the dual-arm robot. This proves efficacy of the proposed optimal control formulation in energy optimal path planing.

Review of various works on the earth-based experimentation for a satellite mounted robotic system has been reported in [24]. It was shown that the scenario of autonomous capture by satellite mounted planar robot can be replicated on earth without much difficulty. Similar earth-based experimental work is also planned for this research work. The planar dual-arm robotic system will be mounted on an air bearing table which will imitate the motion of the base satellite. The dual-arm will be kept in horizontal plane, and hence, its dynamics will not be affected by gravity.

V. Conclusions

Energy optimal path planing strategies to intercept tumbling space objects in a reactionless manner is presented in this work. The reactionless manipulation in task space is presented first using a redundancy formalism for point-to-point manipulation, which allows one to obtain several reactionless paths. Constrained local optimization is presented next to minimize energy consumption. This, however, failed to provide energy optimal path due to dynamic nature of the constrains for reactionless manipulation. In order to overcome this disadvantage, an optimal control problem is formulated. The results showed significant improvement in energy and power consumption. The method ensures reactionless manipulation with minimum energy consumption. The method is illustrated using a 6-DOF planar dual-arm robot. This approach will be extended to a 14-DOF spatial dual-arm robot in future work. Experimental implementation of the proposed method on an earth-based planar dual-arm robot is also planned in future.

References

[1] J. C. Liou, N. Johnson, and N. Hill, Controlling the Growth of Future LEO Debris Populations with Active Debris Removal, Acta Astronautica, 66(56), pp. 648653, 2009.

[2] B. Barbee, S. Alfano, E. Pinon, K. Gold, and D. Gaylor, Design of Spacecraft Missions to Remove Multiple Orbital Debris Objects, IEEE Aerospace Conference, pp. 1-14, 2011.

[3] S. Dubowsky, and M. A. Torres, "Path Planning for Space Manipulators to Minimize Spacecraft Attitude Disturbances," IEEE International Conference on Robotics and Automation, 1991, pp. 2522-2528.

[4] M. A. Torres and S. Dubowsky, "Minimizing Spacecraft Attitude Disturbances in Space Manipulator Systems," Journal of Guidance, Control, and Dynamics, 15(4), pp. 1010-1017, 1992.

[5] D. N. Nenchev and K. Yoshida, "Impact Analysis and Post-impact Motion Control Issues of a Free-floating Space Robot subject to a Force Impulse," IEEE Transactions on Robotics and Automation, 15(3), pp. 548-557, 1999.

[6] K. Yoshida, K. Hashizume and S. Abiko, "Zero Reaction Maneuver: Flight Validation with ETS-VII Space Robot and Extension to Kinematically Redundant Arm," IEEE International Conference on Robotics and Automation, 2001, pp. 441-446.

[7] O. P. Agrawal and Y. Xu, "On the Global Optimum Path Planning for Redundant Space Manipulators,"IEEE Transactions on Man and Cybernetics, pp. 1306-1316. 1994.

[8] R. Lampariello, S. Agrawal, and H. Hirzinger, Optimal Motion Planning for Free-Flying Robots, International Conference on Robotics and Automation, pp. 3029-3035, 2003.

[9] T. Oki, H. Nakanishi and K. Yoshida, Time-Optimal Manipulator Control of a Free-Floating Space Robot with Constraint on Reaction Torque IEEE/RSJ International Conference on Intelligent Robots and Systems, pp. 2828-2833, 2008.

[10] F. Aghili, "Optimal Control for Robotic Capturing and Passivation of a Tumbling Satellite with Unknown Dynamics," AIAA Guidance Navigation and Control Conference, pp. 1-21, 2008.

[11] Z. Ma, O. Ma, B.N. Shashikanth , "Optimal Control for Spacecraft to Rendezvous with a Tumbling Satellite in a Close Range," IEEE/RSJ International Conference on Intelligent Robots and Systems, pp.4109-4114, 2006.

[12] A. Flores-Abad and O. Ma, "Control of a Space Robot for Minimal Attitude Disturbance to the Base Satellite for Capturing a Tumbling Satellite", Proc. SPIE 8385, Sensors and Systems for Space Applications, 83850J, 2012.

[13] P. Huang, J. Yan, J. Yuan and Y. Xu, "Robust Control of Space Robot for Capturing Objects Using Optimal Control Method," IEEE International Conference on Information Acquisition, pp. 397-402, 2007.

[14] P. Huang. K. Chen and Y. Xu, "Optimal Path Planning for Minimizing Disturbance of Space Robot," 9th International Conference on Control, Automation, Robotics and Vision, pp. 1-6, 2006.

[15] S. K. Agrawal and S. Shirumalla, "Planning Motions of a Dual-arm Free-floating Manipulator Keeping the Base Inertially Fixed ", Mechanism and Machine Theory, 30(1), pp. 59-70, 1995.

[16] W. Xu, Y. Liu, and Y. Xu, The Coordinated Motion Planning of a Dual-arm Space Robot for Target Capturing, Robotica, 30(5), pp. 755-771, 2012.

[17] H. Patolia, P. M. Pathak, and S. C. Jain, "Trajectory Control of a Dual-arm Planar Space Robot with Little Attitude Disturbance," SIMULATION, 87(3), pp. 188-204., 2010.

[18] S. V. Shah, A. K. Misra, and I. Sharf, Reactionless Path Planning Strategies for Capture of Tumbling Objects in Space Using a Dual-Arm Robotic System, Accepted for presentation in The AIAA Guidance, Navigation, and Control Conference, Boston, 2013.

[19] D. Dimitrov and K. Yoshida, "Utilisation of Holonomic Distribution Control for Reactionless Path Planning," IEEE/RSJ International Conference on Intelligent Robots and Systems, pp. 3387-3392, 2006.

[20] S. K. Saha, A Unified Approach to Space Robot Kinematics, Transactions on Robotics and Automation, 12(3),401-405, 1996.

[21] J. Angeles, Fundamentals of Robotic Mechanical Systems: Theory, Methods, and Algorithms. Springer, 2007.

[22] S. V. Shah, S. K. Saha, and J. K. Dutt. Dynamics of Tree-Type Robotic Systems. Springer Netherlands, 2013.

[23] P. Rutquist and M. Edvall, PROPT: MATLAB Optimal Control Software. Pullman, US: Tomlab Optimization Inc, 2010.

[24] W. Xu, B. Liang, and Y, Xu. "Survey of Modeling, Planning, and Ground Verification of Space Robotic Systems," Acta Astronautica 68(11), 1629-1649, 2011.